Macromolecules

ARTICLE

pubs.acs.org/Macromolecules

Nanocomposite Materials with Controlled Anisotropic Reinforcement Triggered by Magnetic Self-Assembly

Anne-Sophie Robbes,[†,‡] Fabrice Cousin,[*,†] Florian Meneau,[‡] Florent Dalmas,[§] François Boué,[†] and Jacques Jestin[*,†]

[†]Laboratoire Léon Brillouin, CEA Saclay, 91191 Gif-sur-Yvette Cedex, France

[‡]Synchrotron SOLEIL, L'Orme des Merisiers, PO Box 48, Saint-Aubin, 91192 Gif sur Yvette, France

[§]Institut de Chimie et des Matériaux Paris-Est, CNRS UMR 7182, 2-8 rue Henri Dunant 94320 Thiais, France

ABSTRACT: Nanocomposite materials filled with nanoparticles currently exhibit two important unsolved experimental challenges: (i) the elaboration of a general strategy allowing to finely tune, for an easy-to-tune range of parameters, the anisotropy of nanoparticle assembly inside a polymer matrix for improved anisotropic mechanical reinforcement and (ii) an experimental demonstration establishing that the macroscopic mechanical properties of the materials are quantitatively controlled by the filler microstructure. We address them both here by showing how the versatile bottom-up organization of spherical magnetic nanoparticles controlled by a moderate external magnetic field during processing, enables to obtain a wide variety of anisotropic structures, from quasi-isotropic up to a homogeneous dispersion of aligned chains of nanoparticles, as shown by a refined structural study combining SAXS and TEM experiments. The resulting anisotropy of the mechanical properties is spectacular relative to the low particle volume fraction. The Young modulus can be more than 3 times higher when the bulk material is stretched parallel as opposed to perpendicular to the chains and correlates quantitatively in a proportional manner with the anisotropy of the microstructure.

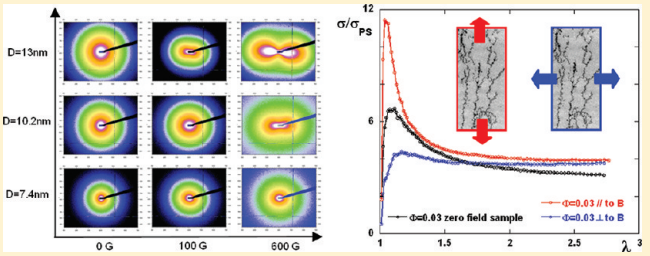

I. INTRODUCTION

It has been known for more than a century that the inclusion of hard particles in a polymer matrix strongly improves their mechanical properties, i.e., their reinforcement and deformability. If the size of the reinforcing particles is decreased down to the nanometer range, the increase of the contact surface between the fillers and the polymer chains strongly enhances such mechanical properties.[1] If a full description of the mechanisms of reinforcement remains to be elucidated, great progress toward the understanding has been accomplished these past years by the design and comprehensive studies of experimental model systems. They have shown the relevance of two main contributions: (i) the first one comes from the local structure and reorganization of the filler network under stretching and is especially important beyond the percolation threshold leading to the fast increase of the Young modulus diverges;[2] (ii) the second one, which is very sensitive to the specific area of the fillers, comes from a modification of the mobility of the chains in the vicinity of the fillers that become "glassy" and behave as an additional rigid phase.[3] The exact balance between these two contributions for the reinforcement mechanisms is still an open question and is very system-dependent. It nevertheless clearly appears that the key point for the design of nanocomposites with dedicated mechanical properties is the control of the morphology of the aggregates at the local scale within the nanocomposite because it acts directly on both contributions. Thus, if one succeeds in tuning and controlling[4] such morphology in an anisotropic and reproducible way, it opens the way to the design of a wide range of new materials with intrinsic anisotropic mechanical properties, ranging from quasi-isotropic reinforcement to pure 1-D reinforcement.

A potential way of producing such an oriented and anisotropic filler network is the use of anisotropic nanoparticles as fillers among the large existing available library of anisotropic nanoparticles, such as carbon nanotubes[5] or fractal carbon black,[6] coming either from nature, such as cellulose whiskers[7] or clays,[8] or from the significant recent progress made in colloidal synthesis. However, this raises two difficulties. First, it is not easy to keep the desired controlled orientation at all concentrations because the anisotropic nanoparticles spontaneously self-orient due to isotropic/nematic or isotropic/smectic transitions. Second, if one wishes to tune the anisotropy of the whole network through the anisotropy of the nanofillers, it is necessary to make as many syntheses as desired anisotropic morphologies, which is very time-consuming and even impossible in the case of some natural compounds.

A promising "bottom-up" route is to start from spherical building nanoblocks and self-assemble them into anisotropic aggregates with a desired anisotropy by an internal trigger tunable over a very wide range of volume fractions. Such strategy consists of grafting the particles with the same polymer that of the matrix

Received: May 12, 2011
Revised: October 11, 2011
Published: October 27, 2011

Scheme 1. Geometry Used during the SAXS Experiments on Anisotropic Samples with Respect to the Direction of the Imposed Magnetic Field in Direct Space and Directions of Averaging of the 2-D SAXS Picture

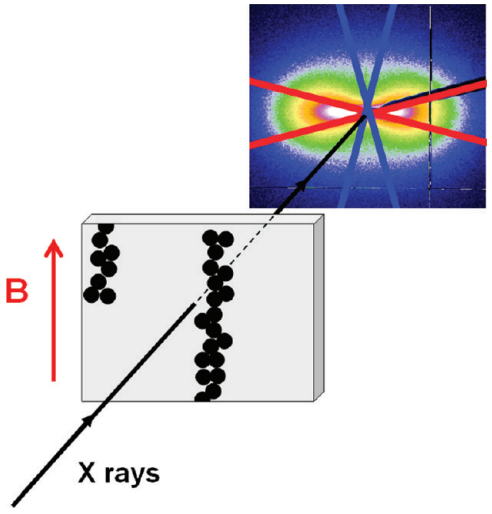

and tuning the anisotropic morphology of the aggregates with the grafting density or with the grafted/free chain length ratio.[9,10] However, a refined synthesis is essential to organize the spherical particles in a controlled way in the entire 3-D bulk material. It remains a complex problem in comparison with controlled 1-D or 2-D arrays of spherical nanoparticles at interfaces[11] or in very thin films.

Thus, an alternative and more flexible route is the use of an external trigger to control the anisotropy, which can be applied during the nanocomposite processing. In this framework we show how the use of an external magnetic field during the processing of a nanocomposite made of polystyrene (PS) chains reinforced by maghemite magnetic nanoparticles (γ-Fe_2O_3) enables us to get a large set of controlled structures by an appropriate choice of both the nanoparticle size and the magnetic field intensity. This rather simple idea of using the magnetic properties of the nanoparticles for the tuning of their aggregation during the processing is reported here for the first time, to the best of our knowledge. Indeed, most of the work concerning the design of polymer composites including magnetic nanoparticles aimed to provide magnetic properties to the material after synthesis.[12] Previously tested for micronic particles,[13−15] the only work where the idea was tested with nanoparticles for dedicated mechanical applications was done by us on latex nanocomposite films on a system based on spherical copolymer nanobeads as building blocks for the polymer part.[16] If this system allowed us to prove unambiguously that the specific reorganizations of the anisotropic network leads to an anisotropic reinforcement, its versatility was restricted due to the numerous chemical steps involved in its synthesis and by it specific mechanical behavior. The system we present here has no such drawbacks. The polymer used can be considered as a classical elastomeric material well above T_g, and both nanoparticles and polymer matrix are easy to purchase or to synthesize in huge quantities and in a reproducible way at low cost. These last points are essential to move from research laboratories to industrial applications. Above all, this simple synthesis enables us to play at will with all the relevant parameters—nanoparticle diameter, filler concentration, and magnetic field intensity—that control the final reinforcement properties.

This system is constituted of a common PS matrix filled with magnetic nanoparticles (γ-Fe_2O_3). Its potential comes from the high sensitivity of the response of the magnetic nanoparticles to an external magnetic field for a small change of size, as the dipolar magnetic interactions are sensitive to the square of the nanoparticles volume. We have shown in ref 17 that, within a probed range of nanoparticles mean diameter D_{mean} lying between 7.4 and 13 nm, the nanoparticles are organized with a reproducible hierarchical structure driven by a two-step aggregation process during casting. Dense primary aggregates composed of some tens of nanoparticles are first formed whatever the volume fraction Φ_{mag}, the diameter of which (∼16 nm) is constant whatever the initial nanoparticle size. For $\Phi_{mag} > 10^{-4}$, these primary aggregates undergo a secondary aggregation step which leads to fractal aggregates of primary aggregate of dimension 1.7, with a radius of ∼200 nm. Although D_{mean} varies only by a factor 2, the expectable behavior under magnetic field can change drastically because the dipolar magnetic interactions, proportional to D_{mean}^6, increase by a factor ∼30 between 7.4 and 13 nm. We thus chose three nanoparticle diameters, denoted S (D_{mean} = 7.4 nm), M (D_{mean} = 10.2 nm), and L (D_{mean} = 13 nm).

The structural study in the absence of magnetic field[17] has allowed us to select three regimes of Φ_{mag} of interest for the processing under magnetic field, with a percolation threshold located between Φ^* = 0.02 and 0.03. We decided to work here at $\Phi_{mag} = 5 \times 10^{-4}$ to probe the influence of magnetic field on the formation of secondary aggregates in the dilute regime and at Φ_{mag} = 0.01 and Φ_{mag} = 0.03 to probe the influence of magnetic field in a concentrated regime, below Φ^* and close to Φ^*.

II. MATERIALS AND METHODS

1. Samples Preparation. The different batches of nanoparticles came from the same synthesis, performed according to the Massart method in aqueous media.[20] The initial batch was then fractioned by a size-sorting process based on gas−liquid colloidal transitions.[21] The size of the nanoparticles, which follow a log-normal distribution, was measured either by SAXS in dilute regime or by magnetization measurements. Both methods give the same results.[17] For nanoparticles S, we obtained D_{mean} = 7.4 nm (d_0 = 6.4 nm; σ = 0.32), for nanoparticles M, D_{mean} = 10.2 nm (d_0 = 8.8 nm; σ = 0.32), and for nanoparticles L, D_{mean} = 13 nm (d_0 = 10.8 nm; σ = 0.32). The aqueous solvent was then exchanged by dialysis with dimethylacetamide (DMAc), a polar solvent which is also a good solvent for the polystyrene (PS).[17] The suspension of maghemite nanoparticles previously in DMAc was then mixed with a concentrated solution of PS in DMAc (10% v/v). We use large polydisperse PS chains for the matrix (M_w 280 000 g/mol, I_p = 2, Aldrich, used as-received). The mixtures were gently stirred for 2 h. They were then poured in a rectangular homemade Teflon mold (3 × 5 cm) and let cast in an oven at constant temperature T_{cast} = 130 °C for 8 days. T_{cast} is much lower than the boiling point of DMAc (160 °C), which ensures gentle evaporation while the medium becomes viscous enough to slow down structure evolution. The volume of mixture poured in the mold was adjusted to get nanocomposites films with a thickness of ∼0.1 cm. This yields dry films of 1.5 cm^3 (3 cm × 5 cm × 0.1 cm). At the final stage, the residual solvent content inside the film was below 1% w/w (0.3 wt % determined by thermogravimetric analysis). For the casting under magnetic field, a constant magnetic field was imposed by two plates of iron magnetized by a series of permanents NeFeB magnets inserted in the mold. The number of permanents magnets inserted in the

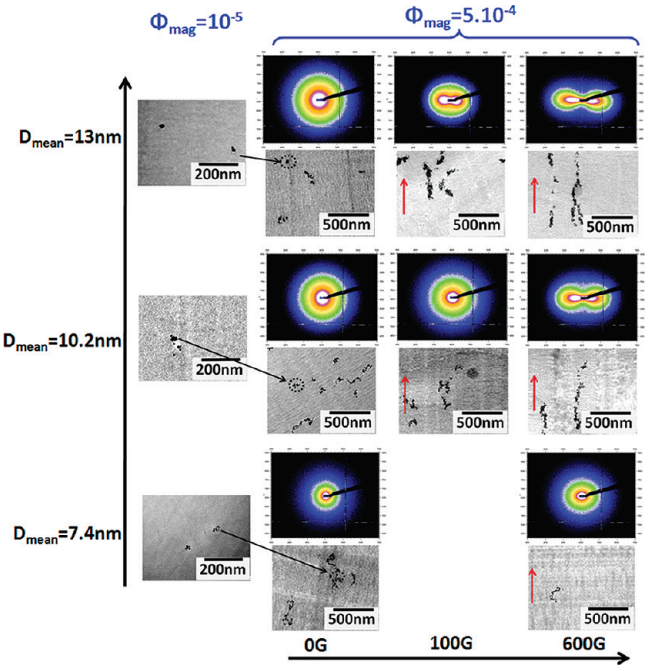

Figure 1. Influence of the magnetic field on the nanoparticle dispersion in dilute regime as a function of the nanoparticles size. 2-D SAXS images in reciprocal space of the nanostructure of the films at $\Phi_{mag} = 5 \times 10^{-4}$ and corresponding TEM images for three nanoparticle sizes (from bottom to top: nanoparticles S (D_{mean} = 7.4 nm), nanoparticles M (D_{mean} = 10.2 nm), and nanoparticles L (D_{mean} = 13 nm) at three magnetic field intensities (from left to right: B = 0 G, B = 100 G, and B = 600 G). The red arrow on the TEM images indicates the direction of the magnetic field. The TEM images of the primary aggregates for the three nanoparticle sizes at $\Phi_{mag} = 10^{-5}$ are shown for information. The sample for nanoparticles S at 100 G has not been synthesized because we assumed that it would not show significant anisotropy.

mold enables to vary the magnetic field up to a maximum value of 600 G. The cartography of the applied field within the mold was done with a Hall effect probe to test its homogeneity. For a desired nominal value of applied field of 600 G, the homogeneity was very satisfactory: the lowest and upper magnetic field measured were respectively 585 and 615 G.

2. SAXS Experiments. The SAXS experiments were carried out at the SWING beamline of the Soleil Synchrotron. Measurements were performed at an energy of 7 keV (λ = 1.77 Å), with a two-dimensional CCD detector placed at a distance of 6.5 and 1.4 m from the sample in order to span a large q-range (q scattering vector, defined by $q = 4\pi \sin(\theta/2)/\lambda$ where θ is the angle between direct beam and scattered beam), ranging from 1.8×10^{-3} to 0.15 Å^{-1}. The scattering of a pure PS matrix, without magnetic nanoparticles, I_{pure_PS}, was first measured. In order to remove the contribution of the PS chains in the films, $(1 - \Phi_{mag})I_{pure\_PS}$ was subtracted from all the nanocomposite samples.

All the samples cast without magnetic field displayed an isotropic structure. The radial averaging was then performed on the entire 2-D detector. All the samples cast under magnetic field displayed an anisotropic structure. They were placed within the X-ray beam so that the direction of the formerly applied magnetic field (during the casting) was vertical (see Scheme 1). All two-dimensional spectra displayed an excess of scattering in the horizontal direction (i.e., transverse to the field). Crudely speaking, this is characteristic of objects elongated vertically, meaning here chains of nanoparticles, aligned parallel to the field. The radial averaging of the 2D spectra was performed inside an angular sector (25°) either along the horizontal direction (red sector) or along the vertical direction (blue sector).

Moreover, a SAXS cartography was performed on an anisotropic sample ($\Phi_{mag} = 5 \times 10^{-4}$, cast with a magnetic field of 600 G) in order to check the homogeneity of the local structure over the whole sample. SAXS data were thus collected every 200 μm in the vertical direction and every 500 μm in the horizontal one, on a surface of 8000 × 4000 μm^2 with a focused X-ray beam of 50 × 300 μm^2. All spectra showed to be similar over the whole surface demonstrating the homogeneity of the structure.

3. Strain−Stress Experiments. Mechanical tests were performed with a homemade uniaxial-elongation machine. Rectangular pieces ($L \times 3L$) are cut from the samples and were polished with sandpaper to obtain a constant thickness. They were stretched up in a controlled constant-rate deformation (γ = 0.005 s^{-1}) at a temperature $T_{str} = T_g$ + 15 °C, where T_g is the glass transition of a given sample. During stretching, samples were placed in silicon oil thermalized by a Lauda bath at T_{str} to ensure a very good thermal homogeneity ($T - T_{str} \leq \pm 1$ °C on a whole given sample). In the range of chosen velocity of deformation and sample size aspect (constant ratio width over length equal to 1/3 before elongation), the macrosocopic homogeneity in deformation through the sample is satisfactory. It is checked after each experiment with the help of a grid drawn on the sample (this indeed is confirmed by SAXS cartography). The T_g was previously determined by differential scanning calorimetry on TA DSC Q100. The T_g of the reference PS matrix is 105 °C, and the T_g's of the other samples are of the same order ±1 °C, whatever the nanoparticle size and concentration. As the precision of the DSC measurements is around 1 °C, there is no modification of T_g when nanoparticles are added. The force $F(\lambda)$, where $\lambda = L/L_0$ defines the elongation with respect to the initial length L_0, was measured with a HBM Q11 force transducer and converted to (real) stress inside the material σ by dividing the force by the assumed cross section during elongation. The deformation of the film was supposed to be homogeneous and incompressible. For the nanocomposites processed under magnetic field, two rectangular films were cut from the same sample and were stretched parallel or perpendicular to the magnetic field. This allowed a direct comparison of the stress−strain isotherms in the two different directions.

4. Transmission Electronic Microscopy. The samples were cut at room temperature by ultramicrotomy using a Leica Ultracup UCT microtome with a diamond knife. The cutting speed was set to 0.2 mm s^{-1}. For the samples synthesized under magnetic field, thin sections were cut with the direction of the magnetic field parallel to the cutting plane. The thin sections of about 40 nm thickness were then floated on deionized water and collected on a 400 mesh copper grid. Transmission electron microscopy was performed on a Tecnai F20 ST microscope (field-emission gun operated at 3.8 kV extraction voltage) operating at 200 kV. Accurate observations of various regimes of the sample were systematically done, starting at a small magnification which was then gradually increased. The sample aspect remained similar on the whole area and for all pieces.

III. RESULTS AND DISCUSSION

1. Tuning of the Structure in a Dilute Regime ($\Phi_{mag} = 5 \times 10^{-4}$). The very high sensitivity of the response of the system to the action of a weak magnetic field during casting, as a function of nanoparticles size, is illustrated in Figure 1. It compares, for different experimental conditions, the 2-D images in reciprocal space of the film structures after casting obtained by small-angle X-ray scattering (SAXS) experiments and the corresponding pictures of the same films obtained by transmission electronic microscopy (TEM). The TEM images of the primary aggregates obtained at $\Phi_{mag} = 10^{-5}$ are shown for information. For the smallest nanoparticles S, the structure obtained for B = 600 G is nearly isotropic while the structure obtained for the largest

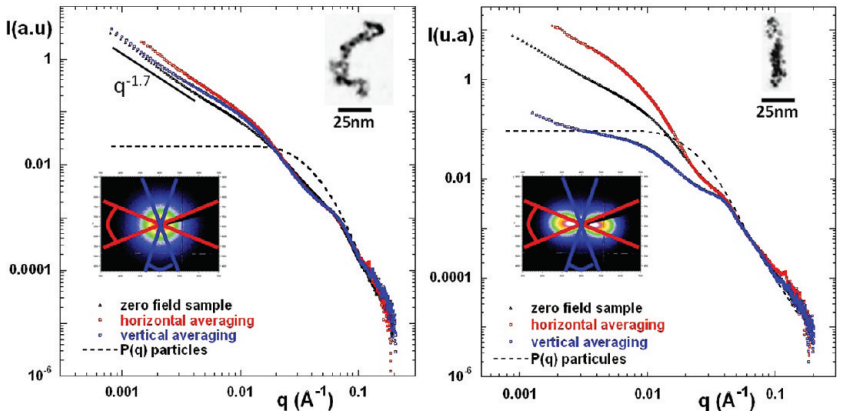

Figure 2. SAXS scattering spectra of films at $\Phi_{mag} = 5 \times 10^{-4}$ cast under an applied magnetic field of 600 G for (a) nanoparticles S ($D_{mean} = 7.4$ nm) and (b) nanoparticles L ($D_{mean} = 13$ nm). Red curves correspond to the horizontally averaged scattering (angular radial averaging of 25°). Blue curves correspond to the vertically averaged scattering (angular radial averaging of 25°). Black curves correspond to isotropic samples synthesized without an applied magnetic field. The dashed lines correspond to the form factor of the nanoparticles. Corresponding 2D-SAXS images and TEM images are presented in the inset for information.

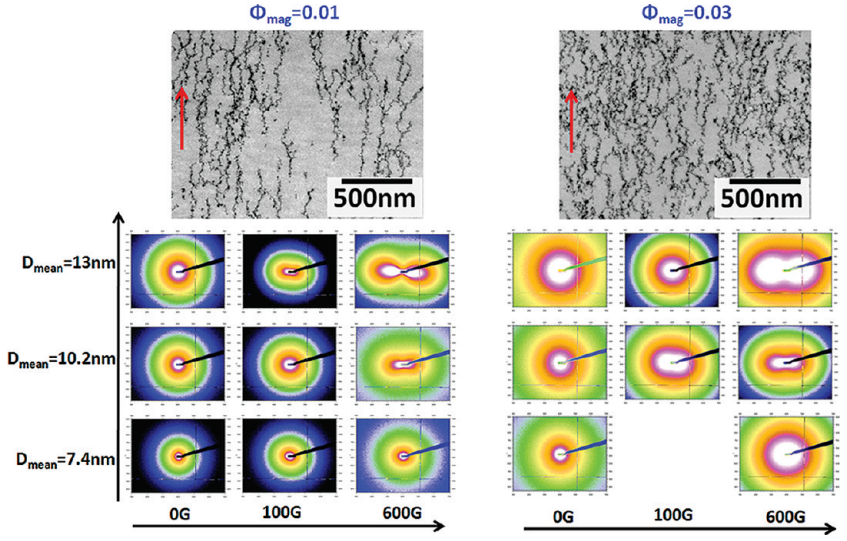

Figure 3. Influence of the magnetic field on the nanoparticle dispersion in two concentrated regimes as a function of the nanoparticle size. 2-D SAXS images in reciprocal space of the nanostructure of the films at $\Phi_{mag} = 0.01$ (left) and $\Phi_{mag} = 0.03$ (right) for three nanoparticle mean diameters (from bottom to top: nanoparticles S ($D_{mean} = 7.4$ nm), nanoparticles M ($D_{mean} = 10.2$ nm), and nanoparticles L ($D_{mean} = 13$ nm) at three magnetic fields (from left to right: $B = 0$ G, $B = 100$ G, and $B = 600$ G). Corresponding TEM images of films at $\Phi_{mag} = 0.01$ and $\Phi_{mag} = 0.03$ for nanoparticles L ($D_{mean} = 13$ nm) synthesized under a 600 G magnetic field are presented. The red arrow indicates the direction of the applied magnetic field. The sample corresponding to the film made of nanoparticles S ($\Phi_{mag} = 0.03$) at 100 G is missing because we assumed that it would not show significant anisotropy.

nanoparticles L at the same intensity of magnetic field is strongly anisotropic. It reveals the strong orientation of the aggregates along the field in film. Between these two extremes, a series of anisotropic structures is obtained with increased anisotropy, whether the nanoparticle size or the magnetic field during casting is increased. It proves that the process enables us to obtain films with a chosen anisotropic structure by an appropriate selection of the experimental parameters prior to casting.

In order to get a better insight on such anisotropic structures, we compare in Figure 2 the scattering curves of the two extreme cases, i.e., the films for nanoparticles S and L without and with an applied magnetic field of 600 G. Without magnetic field, the structures can be described as follows:[17] at large q, they superimpose with the form factor of the nanoparticles. Going toward slightly lower q (respectively at 0.08 $Å^{-1}$ for nanoparticles S and 0.05 $Å^{-1}$ for nanoparticles L), there is a shoulder in the curve corresponding, in direct space, to the contact between two nanoparticles inside the primary aggregate. At lower q, one probes then the form factor of the primary aggregates down to ~0.01 $Å^{-1}$; at this value there is a break of slope corresponding, in direct space, to the contact between two primary aggregates. Finally, for $q < 0.01$ $Å^{-1}$, the scattering decays as $q^{-1.7}$ since the primary aggregates are organized in secondary fractal aggregates of dimension 1.7.

For the nanoparticles S at 600 G, both horizontally averaged and vertically averaged scattering are similar to the one without a magnetic field, down to 0.01 $Å^{-1}$. It means that the formation of primary aggregates is not disturbed by the field. A moderate

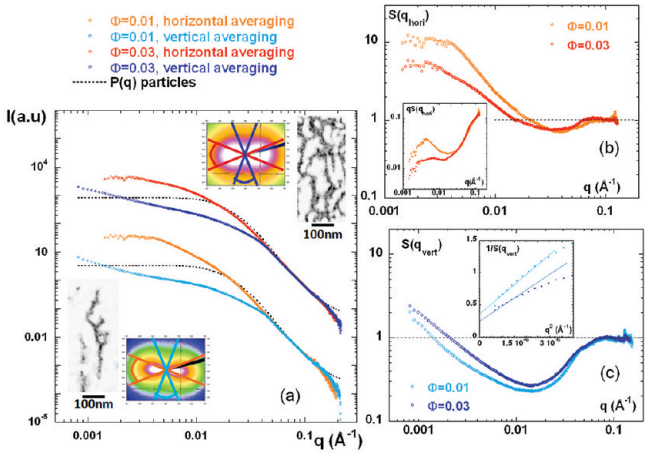

Figure 4. (a) SAXS scattering spectra of nanoparticles L inside the films at $\Phi_{mag} = 0.01$ and $\Phi_{mag} = 0.03$ cast under an applied magnetic field of 600 G. Red curves correspond to the horizontally averaged scattering (angular radial averaging of 25°). Blue curves correspond to the vertically averaged scattering (angular radial averaging of 25°). The dashed lines correspond to the form factor of the nanoparticles. Corresponding 2D-SAXS images and TEM images are presented in the inset for information. (b) Comparison of the structure factor $S(q_{hori})$ with nanoparticles L at $\Phi_{mag} = 0.01$ and $\Phi_{mag} = 0.03$; in inset: $qS(q_{hori}) = f(q)$. (c) Comparison of the structure factor $S(q_{vert})$ with nanoparticles L at $\Phi_{mag} = 0.01$ and $\Phi_{mag} = 0.03$; in inset: $1/S(q)_{vert} = f(q^2)$.

anisotropy appears at low q, showing a very weak alignment of primary aggregates during secondary aggregation as confirmed by TEM experiments. But the slope of the scattering decay remains very close to the 0 G case. On the contrary, the scattering is very different for the nanoparticles L at 600 G: the vertically averaged scattering is much weaker than the zero-field sample; it resembles the form factor of a primary aggregate measured in the isotropic case at very low Φ_{mag}. The interparticle correlation shoulder (from inside the primary aggregate) at 0.05 $Å^{-1}$ is visible; the Guinier plateau is reached around 0.01 $Å^{-1}$, showing absence of any further visible correlation between primary aggregates along the direction. On the contrary, the horizontally averaged scattering keeps increasing when going toward low q, down to the lowest q probed in the experiment; a $q^{-1.4}$ power law is seen below the shoulder. Note in particular the vanishing of the break of slope at 0.01 $Å^{-1}$, observed in the 0 G case due to a contact distance between two primary aggregates, which cannot be distinguished anymore here. This very specific behavior can be well understood with the help of the TEM experiments: we see rodlike chains inside which primary aggregates are arranged without any correlations, extending up to a micrometer size along the field. Since some parts of these chains are not completely aligned, their nonzero projection on the horizontal axis can give a rodlike contribution. (The projection x_{ij} of the vectors r_{ij} between two particles i and j along the horizontal direction x will have a contribution $q_x \cdot x_{ij}$ in the $\mathbf{q} \cdot \mathbf{r}_{ij}$ terms of the scattered intensity.) This may correspond to relatively large distances even for small misalignment since the chains are very long. Along this horizontal direction the interchains distances are much larger than their lateral size, such that we can consider that we are in dilute case. Along the vertical direction on the contrary, the very long rods completely overlap: we are above the overlapping concentration, even at such weak volume fraction, and the inner scattering from one chain cannot be seen. This striking consequence of the rod length is seen for a range of directions along the vertical one, which results in the "horizontal eight" (∞) shape of the two-dimensional pattern. It is not observed when the chains are short (S particles at 600 G or M particles at 100 G), for which the patterns are ellipses (the anisotropy is also weak).

For the largest nanoparticles, despite the strong anisotropy of the scattering, the shoulder corresponding to the contact between two nanoparticles is still visible. It suggests that the formation of the rods results from the competition between the formation of isotropic primary aggregates and the chaining of nanoparticles, induced by the dipolar magnetic interactions during casting.

2. Tuning of the Structure in a Concentrated Regime. The fine-tuning of the anisotropy of the nanocomposite structures, which increases either with the intensity of the magnetic field or with the nanoparticle size, extends to the concentrated regime. Figure 3 presents a full complete series of 2-D images, in the reciprocal space, of the structures of the films at $\Phi_{mag} = 0.01$ and $\Phi_{mag} = 0.03$. For such high Φ_{mag}, the chaining of nanoparticles induced by the dipolar magnetic interactions is then the dominant process of aggregation during casting because the primary aggregation almost disappears. This is shown by the TEM images of nanoparticles L at 600 G, which present locally chains of individual nanoparticles.

This anisotropic structure is also clear from the scattering in Figure 4a. The "horizontal eight" (∞) shape is seen also here except for particles S and M at 100 G, for which chains stay short enough even at this concentration. We present the horizontally averaged and vertically averaged scattering of the 2D spectra of the film of nanoparticles L at 600 G at $\Phi_{mag} = 0.01$ and $\Phi_{mag} = 0.03$. We have checked that for all q the scattered intensity decreases continuously from horizontal direction (at 0° with respect to the horizontal axis) to the vertical one. Along a direction, over the whole q range, there is no maximum neither, showing no privileged distance. In order to gain a better insight into the structure, we present in Figure 4b,c the structure factor $S(q)$ of the nanoparticles, i.e., the scattered intensity divided by the form factor of the nanoparticles, in both directions. On both $S(q)$, the shoulder at 0.05 $Å^{-1}$ corresponding to the contact between two nanoparticles has almost vanished, showing that the nanoparticles do not aggregate the same way as formerly in primary aggregates. For $S(q_{hori})$, their decay function remains close to q^{-1} on almost 1 decade down to 0.003 $Å^{-1}$ for $\Phi_{mag} = 0.03$, again possibly due to 1-D chains of the aggregates not completely aligned with the field. For $\Phi_{mag} = 0.01$, this q^{-1} decay is obtained on a narrower range since the $S(q_{hori})$ bends to a $q^{-1.7}$ behavior at low q, showing that the structure is more ramified at large scale. At lower q, $S(q_{hori})$ bends down toward a finite size: the rodlike nature of chaining cannot be seen at larger scale. It corresponds to a finite number of particles equal to 10 for $\Phi_{mag} = 0.01$ and 4 for $\Phi_{mag} = 0.03$. Such typical lengths are also confirmed by the TEM images of Figure 3.

Looking now along the vertical direction, as before the scattering is very low (strongly screened) at intermediate q. Thus, the structure factor $S(q_{vert})$ shows a deep correlation hole, but it is followed at the lowest q's by a strong increase of the intensity, showing large fluctuations of the global concentration along this direction. Though it concerns very large distances, a correlation size of fluctuations ξ can be extracted, with a value of 800 Å for $\Phi = 0.03$, assuming that $S(q) = 1/(1 + q^2\xi^2)$, as demonstrated by the linearity of the Orstein−Zernike plot of $1/S(q_{vert})$ versus q^2 at low q. ξ has a rather limited value, showing that the system stays homogeneous at even larger scale, in

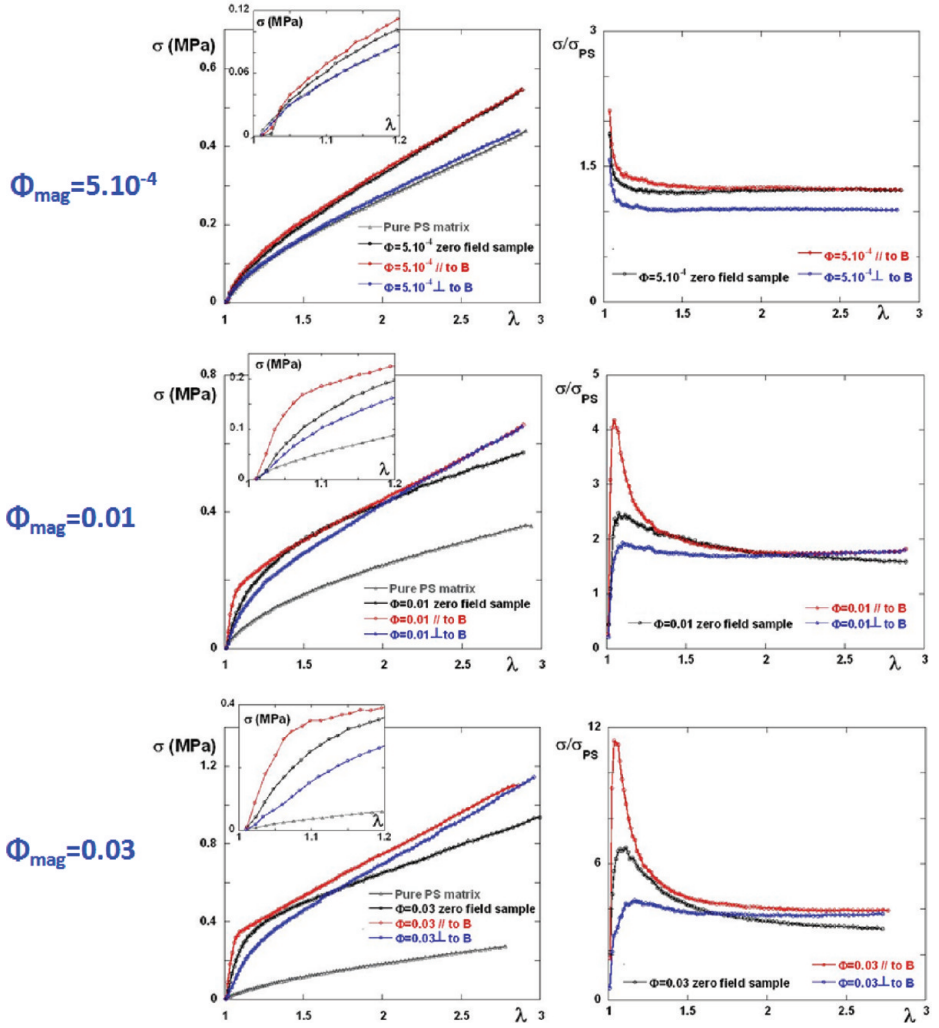

Figure 5. Real stress (on the left) and reinforcement factor σ/σ_{matrix} (on the right) as a function of the elongation λ of nanocomposite films, synthesized with nanoparticles L with and without an applied magnetic field of 600 G at, from bottom to top: (a) $\Phi_{mag} = 5 \times 10^{-4}$, (b) $\Phi_{mag} = 0.01$, and (c) $\Phi_{mag} = 0.03$. Black curves: nanocomposites synthesized without a magnetic field. Red curves: nanocomposites stretched parallel to the applied magnetic field. Blue curves: nanocomposites stretched in the direction perpendicular to the magnetic field. Gray curves: pure PS matrix. Inset: zoom on the linear part of the real stress as a function of the elongation ratio λ, for a better insight. The experiments have been performed at T_g + 15 °C.

accordance with the TEM image. For $\Phi_{mag} = 0.01$, ξ has a value of 1000 Å, which is of the same order as for $\Phi_{mag} = 0.03$.

3. Mechanical Properties. The tuning of the anisotropy of the structure provides a wide variety of anisotropic mechanical behaviors. The most spectacular are obtained for nanoparticles L, as shown in Figure 5. It presents the reinforcement factor σ/σ_{matrix} deduced from the strain−stress isotherms of the nanocomposite films as a function of the particle content, stretched in the direction either parallel to the applied magnetic field or perpendicular to it. It is compared to the isotropic case and to the pure PS matrix. At $\Phi_{mag} = 5 \times 10^{-4}$ (Figure 5a), for which we obtained the rodlike structures of primary aggregates, the reinforcement remains moderate. It is nevertheless quasi-1-D. When the sample is stretched in the direction of the rods, the reinforcement factor is slightly higher to the one of the isotropic case, while in the perpendicular case, the reinforcement remains lower and close to the one of the PS matrix.

In the concentrated regime, the reinforcement is important and strongly anisotropic. In the isotropic case, σ/σ_{matrix} shows a clear maximum around $\lambda = 1.2$ whose amplitude is directly dependent on the volume fraction from 2.5 at $\Phi_{mag} = 0.01$ to 6.5 at $\Phi_{mag} = 0.03$. In the anisotropic samples, the maximum at low λ is marked when stretched parallel to the field at $\Phi_{mag} = 0.01$ and very sharp at $\Phi_{mag} = 0.03$. The system behaves as a connected network in the direction of the alignment of the nanoparticle chains. As the position of the maximum is identical for both concentrations, whereas its amplitude increases almost linearly with the volume fraction, it may well correspond to the simultaneous break of 1-D aggregates of nanoparticle chains whose number is proportional to the volume fraction. This situation stands for the formation of a 1-D connected network, where the rupture points are reduced compared to the classical 3-D filler network. In addition, the slow decrease of the reinforcement factor with the elongation indicates that specific orientation correlations occur between the broken chains in the magnetic field direction. It enables to maintain a residual significant stress even for larger deformations.[16] The maximum on the reinforcement does not exist when stretched perpendicular to the field. The system behaves thus here like a dilute system. At large deformation, σ/σ_{matrix} tends to a plateau with a value higher than

dx.doi.org/10.1021/ma201096u |*Macromolecules* 2011, 44, 8858–8865

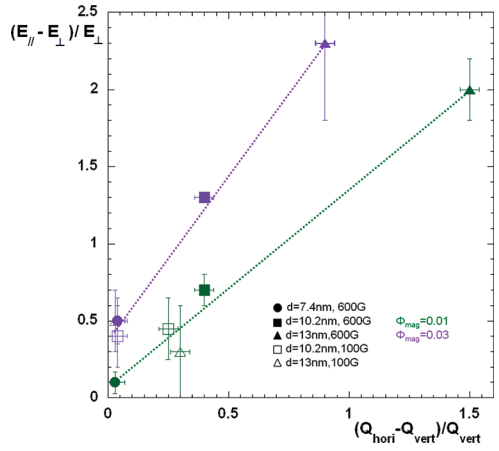

Figure 6. Quantitative correlation of the anisotropy of the macroscopic mechanical properties with the anisotropy of the local structure of the fillers for all samples at Φ_{mag} = 0.01 and Φ_{mag} = 0.03 casted under a magnetic field.

1, corresponding to a remaining stress which could be attributed to the modification of the dynamic of the chains in the vicinity of the nanoparticles,[3] even if it concerns a small number of implicated chains.[18] At low deformation, the strong differences of mechanical behaviors between the two cases arise from the local rearrangement of the chains of nanoparticles under stretching. This leads to their progressive blocking, a process that only occurs when the stretching is performed parallel to the oriented chains, as depicted in ref 16. In such a regime of low deformation, the isotropic case appears to be an average between the parallel and perpendicular cases. At large deformation, the two σ/σ_{matrix} curves from the stretching parallel and the stretching perpendicular to the field converge to the same value. The system is indeed essentially sensitive to the contribution of the mobility of the polymeric chains in this regime of deformation, as explained for the isotropic case. The value of the plateau is slightly larger for the samples processed under a magnetic field. It is due to the larger specific area of the fillers, for a constant introduced Φ_{mag}, because chains of individual nanoparticles replace primary aggregates.

4. Quantitative Correlation between Macroscopic Anisotropic Reinforcement and Local Anisotropic Filler Structure. Finally, we demonstrate the versatility of the system offered by refined combinations of nanoparticles size/magnetic field/volume fraction of the fillers for controlling both the anisotropy and the strength of reinforcing properties. We correlate in Figure 6 the anisotropy of the macroscopic mechanical properties with the anisotropy of the local structure of the fillers, *for all of the samples* synthesized at Φ_{mag} = 0.01 and Φ_{mag} = 0.03 under a magnetic field. To quantify the anisotropy of the mechanical properties of a given sample, we extract its Young modulus in the parallel direction $E_{\parallel}$ and in the perpendicular direction $E_{\perp}$ from the linear regime of the strain−stress isotherms to calculate $(E_{\parallel} - E_{\perp})/(E_{\perp})$. A value equals to zero corresponds to isotropic mechanical properties. The determination of the structural anisotropy is more difficult because the anisotropy of the scattering curves is q-dependent. We thus considered $Q = \int I(q)q^2\,dq = 2\pi^2\phi_{mag}(1 - \phi_{mag})(\rho_{mag} - \rho_{PS})^2$, where ρ_{mag} and ρ_{PS} are respectively the scattering length densities of maghemite and PS,[19] which is the pendent along one direction of the scattering invariant usually averaged over three dimensions. The overall anisotropy of the structure can thus be estimated through $(Q_{hori} - Q_{vert})/(Q_{vert})$ and can be related to the effective volume fractions, i.e., to volume fractions of orientated aggregates, in both directions as $\sim(\Phi_{mag,\parallel} - \Phi_{mag,\perp})/(\Phi_{mag,\perp})$. $(Q_{hori} - Q_{vert})/(Q_{vert})$ increases either with the nanoparticles size or with the applied magnetic field. It illustrates the fact that the structural anisotropy is mainly governed by the dipolar interactions between the nanoparticles.

Remarkably, Figure 6 shows that, for a given Φ_{mag}, all the data of $(E_{\parallel} - E_{\perp})/(E_{\perp})$ versus $(Q_{hori} - Q_{vert})/(Q_{vert})$ from the different samples are superimposing onto the same straight curve. As the Young modulus varies, to a first order, proportionally with the volume fraction, the tuning of the structural local anisotropy is directly converted into a macroscopic anisotropy of the mechanical properties. The slope of the curve increases with an increase of Φ_{mag}. This arises from the fact that transverse correlations between aligned chains of particles, which increase with Φ_{mag}, systematically correlate with stronger anisotropic reinforcement.

Such quantitative correlation is a real breakthrough for both the processing of nanocomposites and the understanding of the relationship between the local filler nanostructure and the macroscopic properties of the material. From an application point of view, it opens the way for the design of new kinds of material, for which the expected properties for a given application can be quantitatively predicted. It will enable the optimization of the choice of the parameters governing the final material (size of nanoparticles, filler content, applied field intensity, etc.). From a fundamental point of view, such quantitative correlation will permit to enhance the current macroscopic mechanical models by providing the relevant spatial length scale of such nanostructures.

AUTHOR INFORMATION

Corresponding Author

*E-mail: fabrice.cousin@cea.fr (F.C.), jacques.jestin@cea.fr (J.J.).

ACKNOWLEDGMENT

The authors are indebted to Sébastien Gautrot for the realization of the mold enabling the casting under magnetic field, to Régine Perzynski for fruitful discussions, and to Natalie Malikova for her careful reading of the manuscript. We thank CEA and Synchrotron Soleil for PhD grant of A. S. Robbes.

REFERENCES

(1) Jordan, J.; Jacob, K.-I.; Tannenbaum, R.; Sharaf, M. A.; Jasiuk, I. *Mater. Sci. Eng., A* **2005**, *393*, 1–11.

(2) Klüppel, M.; Heinrich, G. *Rubber Chem. Technol.* **1995**, *68*, 623–651.

(3) Berriot, J.; Montes, H.; Lequeux, F.; Long, D.; Sotta, P. *Macromolecules* **2002**, *35*, 9756–9762.

(4) Mackay, M.-E.; Tuteja, A.; Duxbury, P. M.; Hawker, C. J.; Van Horn, B.; Guan, Z.; Chen, G.; Krishnan, R.-S. *Science* **2006**, *311*, 1740–1743.

(5) Dalmas, F.; Cavaillé, J.-Y.; Gauthier, C.; Chazeau, L.; Dendievel, R. *Compos. Sci. Technol.* **2007**, *67*, 829–839.

(6) Heinrich, G.; Klüppel, M.; Vilgis, T.-A. *Curr. Opin. Solid State Mater.Sci.* **2002**, *6*, 195–203.

(7) Wang, Y.-Z.; Zhang, L.-Q.; Tang, C.-H.; Yu, D.-S. *J. Appl. Polym. Sci.* **2000**, *78*, 1879–1883.

(8) Favier, V.; Chanzy, H.; Cavaillé, J.-Y. *Macromolecules* **1995**, *28*, 6365–6367.

(9) Akcora, P.; Liu, H.; Kumar, S.-K.; Moll, J.; Li, Y.; Benicewicz, B.-C.; Schadler, L.-S.; Acehan, D.; Panagiotopoulos, A.-Z.; Pryamitsyn, V.;

Ganesan, V.; Ilavsky, J.; Thiyagarajan, P.; Colby, R.-H.; Douglas, J.-F. *Nature Mater.* **2009**, *8*, 354–359.

(10) (a) Chevigny, C.; Dalmas, F.; Di Cola, E.; Gigmes, G.; Bertin, D.; Boué, F.; Jestin, J. *Macromolecules* **2011**, *44* (1), 122–133. (b) Chevigny, C.; Jestin, J.; Gigmes, G.; Schweins, R.; Di Cola, E.; Dalmas, F.; Bertin, D.; Boué, F. *Macromolecules* **2010**, *43* (11), 4833–4837.

(11) Sahoo, Y.; Cheon, M.; Wang, S.; Luo, H.; Furlani, E.-P.; Prasad, P.-N. *J. Phys. Chem. B* **2004**, *108* (11), 3380–3383.

(12) Coquelle, C.; G. Bossis, G. *Int. J. Solids Struct.* **2006**, *43*, 7659 (2006).

(13) Fragouli, D.; Buonsanti, R.; Bertoni, G.; Sangregorio, C.; Innocenti, C.; Falqui, A.; Gatteschi, D.; Davide Cozzoli, P.; Athanassiou, A.; Cingolani, R. *ACS Nano* **2010**, *4* (4), 1873–1878.

(14) Martin, J.-E.; Venturini, E.; Odinek, E.; Anderson, R. A. *Phys. Rev. E* **2000**, *61*, 2818–2830.

(15) Fang, W.-X.; He, Z.-H.; Xu, X.-Q.; Mao, Z.-Q.; Shen, H. *EPL* **2007**, *77*, 68004.

(16) Jestin, J.; Cousin, F.; Dubois, I.; Ménager, C.; Oberdisse, J.; Schweins, R.; Boué, F. *Adv. Mater.* **2008**, *20* (13), 2533–2540.

(17) Robbes, A.-S.; Jestin, J.; Meneau, F.; Dalmas, F.; Sandre, O.; Perez, J.; Boué, F.; Cousin, F. *Macromolecules* **2010**, *43* (13), 5785–5796.

(18) Jouault, N.; Dalmas, F.; Said, S.; Di Cola, E.; Schweins, R.; Jestin, J.; Boué, F. *Phys. Rev. E* **2010**, *82*, 031801.

(19) Spalla, O.; Lyonnard, S.; Testard, F. *J. Appl. Crystallogr.* **2003**, *36* (2), 338–347.

(20) Massart, R. *IEEE Trans. Magn.* **1981**, *17*, 1247.

(21) Massart, R.; Dubois, E.; Cabuil, V.; Hasmonay., E. *J. Magn. Magn. Mater.* **1995**, *149*, 1–5.